

# Promotion Mechanisms of LiBH<sub>4</sub> Dehydrogenation Dominated by Charge Redistribution

Weijie Yang<sup>ab\*</sup>, Han Ge<sup>ab</sup>, Tongao Yao<sup>ab</sup>, Qiyong Chen<sup>ab</sup>, Feiyang Liu<sup>ab</sup>, Mingye Huang<sup>ab</sup>, Junwei Sun<sup>c</sup>, Shuai Dong<sup>ab</sup>, Yanfeng Liu<sup>ab</sup>, Zhengyang Gao<sup>ab</sup>

<sup>a</sup> Department of Power Engineering, North China Electric Power University, Baoding 071003, Hebei, China

<sup>b</sup> Hebei Key Laboratory of Low Carbon and High-Efficiency Power Generation Technology, North China Electric Power University, Baoding 071003, Hebei, China

<sup>c</sup> Guoneng Nanjing Electric Power Test & Research Limited

\* Corresponding author:

Weijie Yang ([yangwj@ncepu.edu.cn](mailto:yangwj@ncepu.edu.cn))

**Table. S1** Comparison of LiBH<sub>4</sub> lattice parameters in different literatures with this study

Lattice parameters	a (Å)	b (Å)	c (Å)
Ref <sup>1</sup>	7.173	4.434	6.798
Ref <sup>2</sup>	7.140	4.290	6.850
Ref <sup>3</sup>	7.179	4.437	6.803
This work	7.141	4.431	6.748

**Table. S2** K-point parameter convergence test

k-points	Energy (Hartree)	delte E	Judgment criteria
1 1 1	-50.6701286544		$ \Delta E  < 3.7 \text{ E-}5$
2 2 2	-50.7413257909	-0.0711971364	
3 3 3	-50.7403112341	0.0010145568	
4 4 4	-50.7403822759	-0.0000710418	
5 5 5	-50.7403802078	<b>0.0000020681</b>	
6 6 6	-50.7403785245	0.0000016833	

**Table. S3** Cutoff parameter convergence test

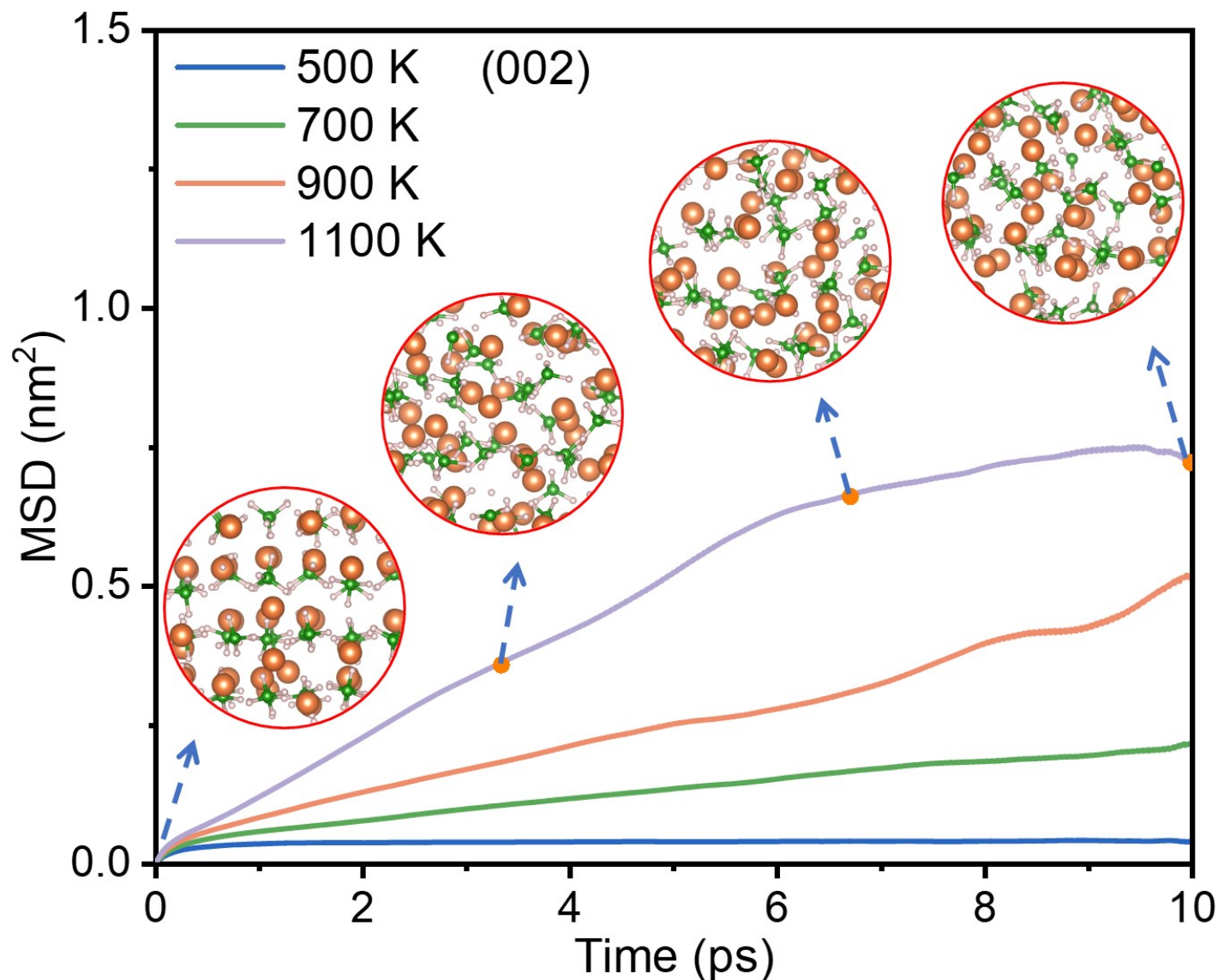
Cutoff (Ry)	Energy (Hartree)	delte E	Judgment criteria
100	-48.5668527094		$ \Delta E  < 1 \text{ E-}6$
150	-48.5214733688	0.0453793406	
200	-48.5007221546	0.0207512142	
250	-48.5002418168	0.0004803378	
300	-48.5001332759	0.0001085409	
350	-48.5001273850	0.0000058909	
400	-48.5001276498	<b>-0.0000002648</b>	

**Table. S4** The expansion multiples of different surfaces and the test values of cutoff and rel-cutoff

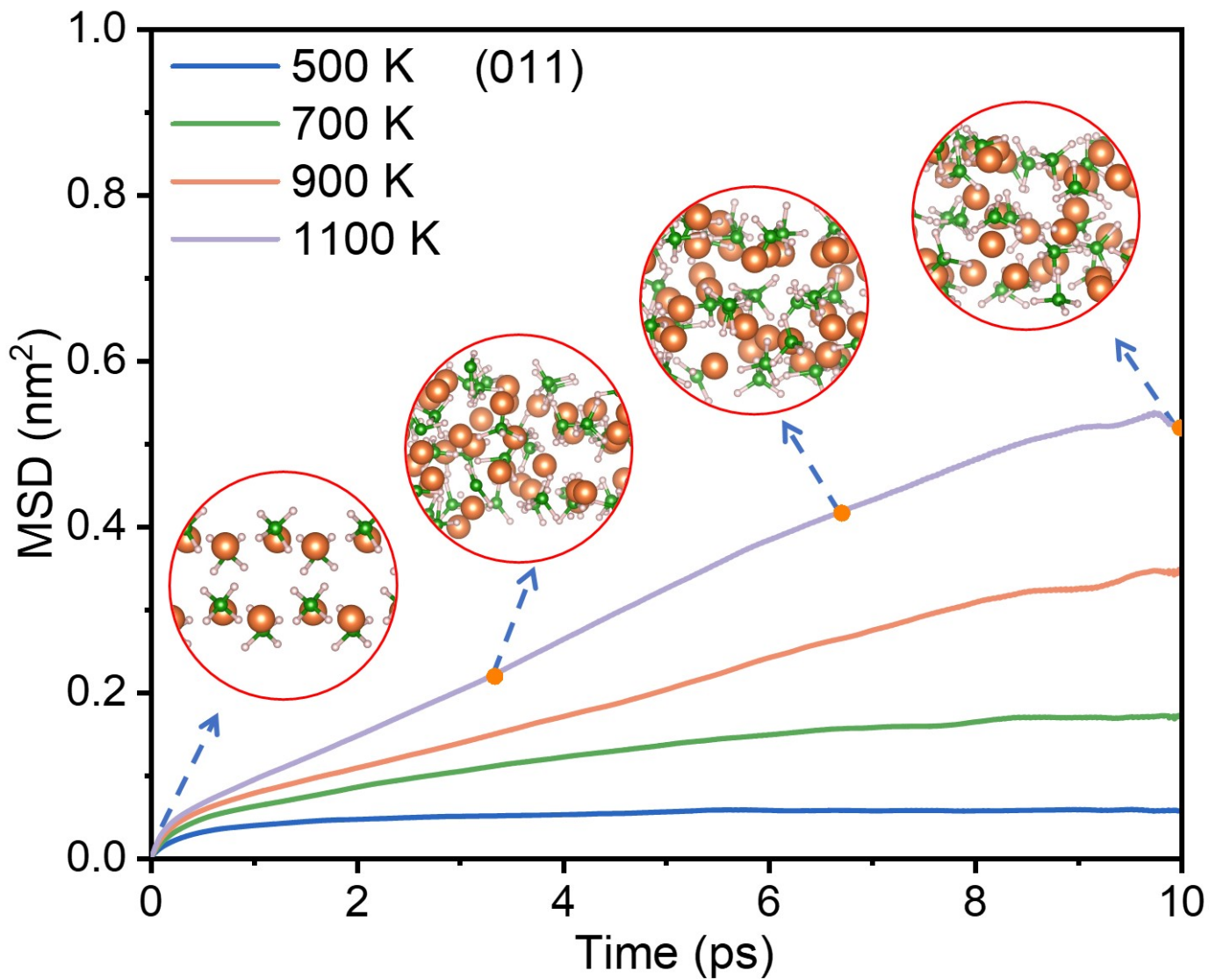
surface	cell expansion multiples	cutoff (Ry)	rel-cutoff (Ry)
(002)	241	700	60
(020)	321	650	70
(011)	331	700	60
(200)	331	800	50
(101)	251	1000	50
(111)	331	550	60

**Table. S5** Crystal cell parameters and atomic counts after expansion for the six different surfaces of LiBH<sub>4</sub>

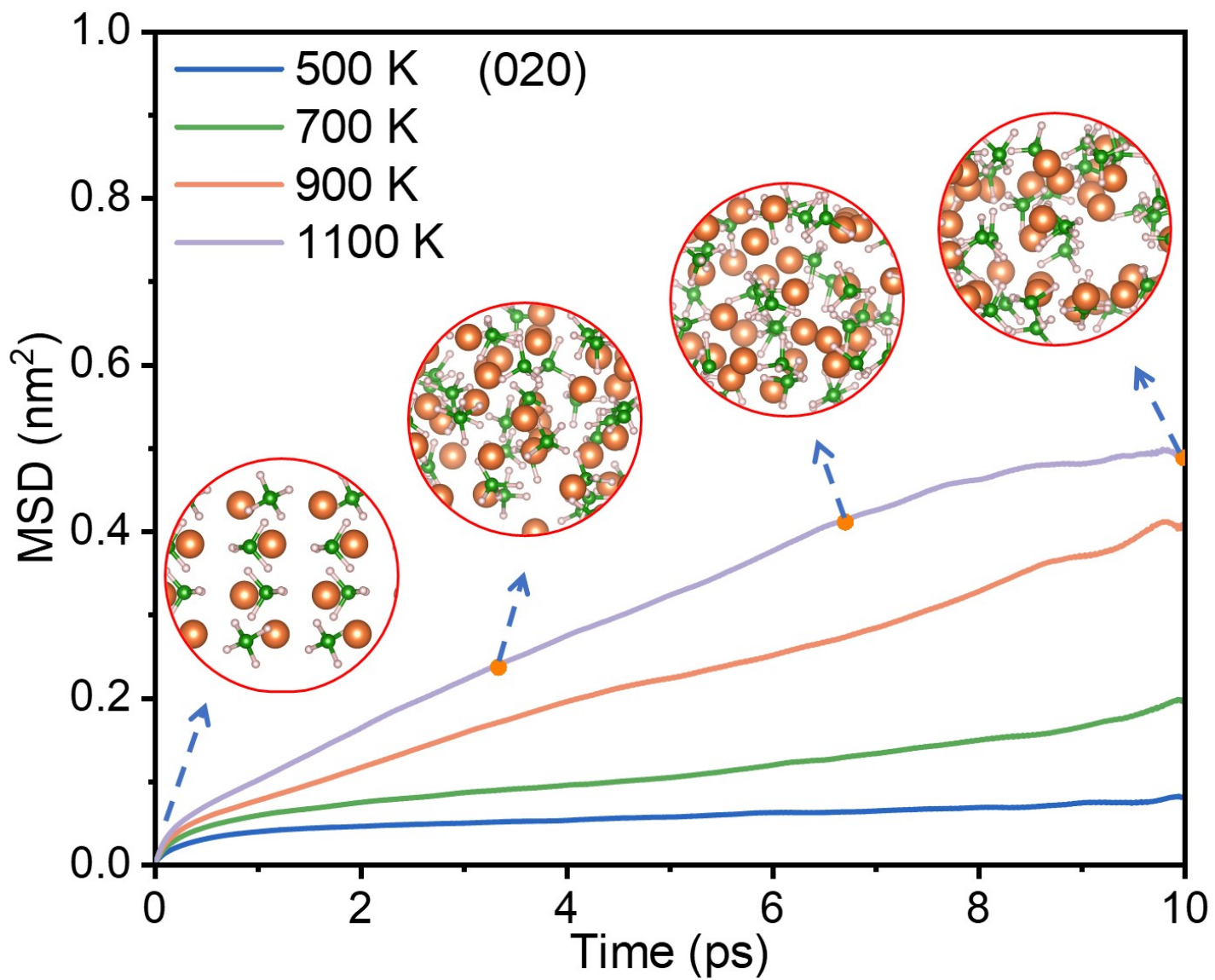
surface	a (Å)	b (Å)	c (Å)	$\alpha$ (°)	$\beta$ (°)	$\gamma$ (°)	number of atoms	cell type
(002)	14.282	17.724	32.960	90	90	90	384	orthorhombic
(020)	20.244	14.282	24.357	90	90	90	288	orthorhombic
(011)	21.423	24.218	21.362	90	90	90	432	orthorhombic
(200)	13.292	20.244	31.908	90	90	90	432	orthorhombic
(101)	19.650	22.155	23.850	90	90	90	480	orthorhombic
(111)	25.2121	24.2182	26.223	90	90	106.82	432	monoclinic



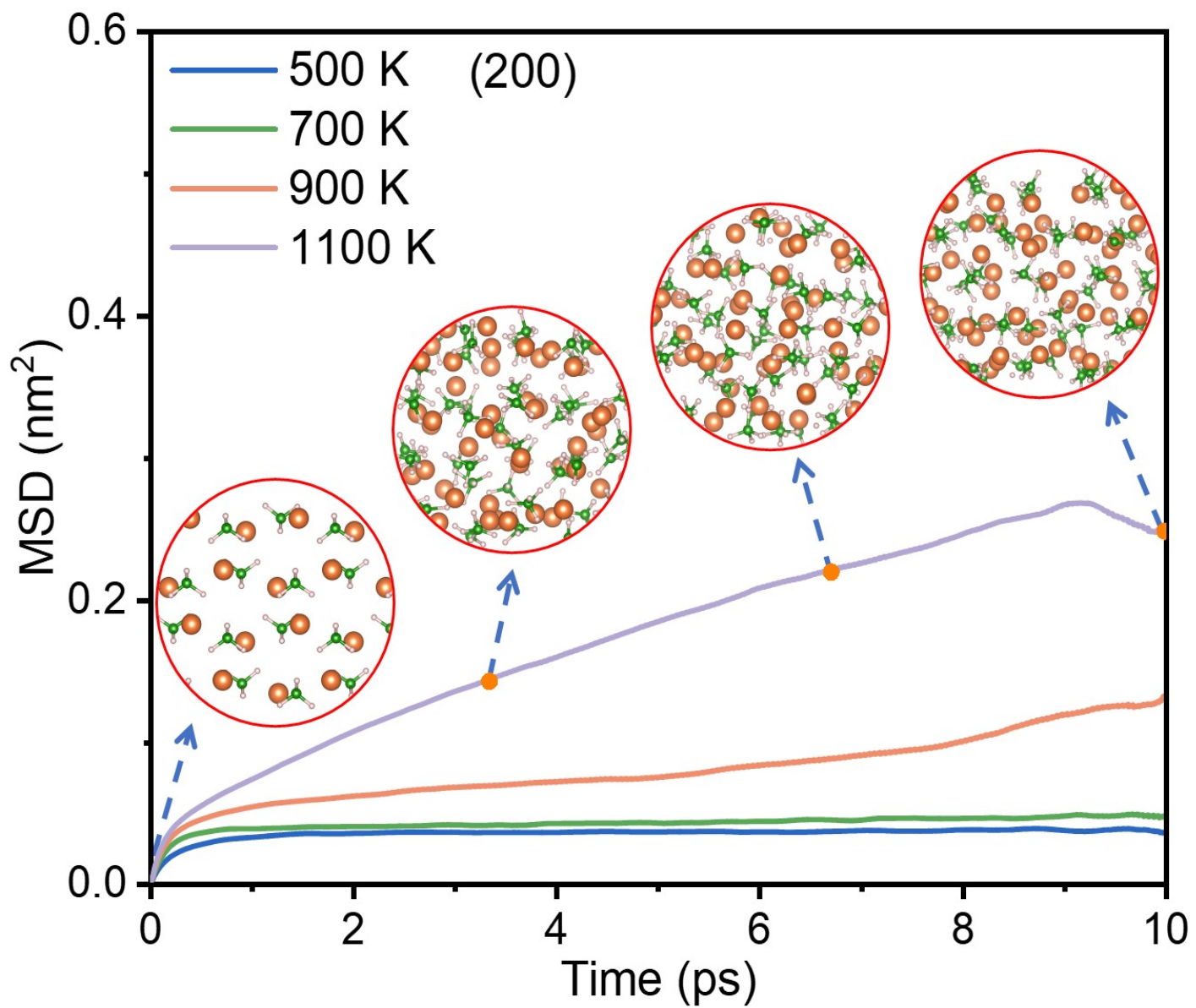
**Fig. S1** The MSD changes of hydrogen atoms at different temperatures for the LiBH<sub>4</sub> (002).



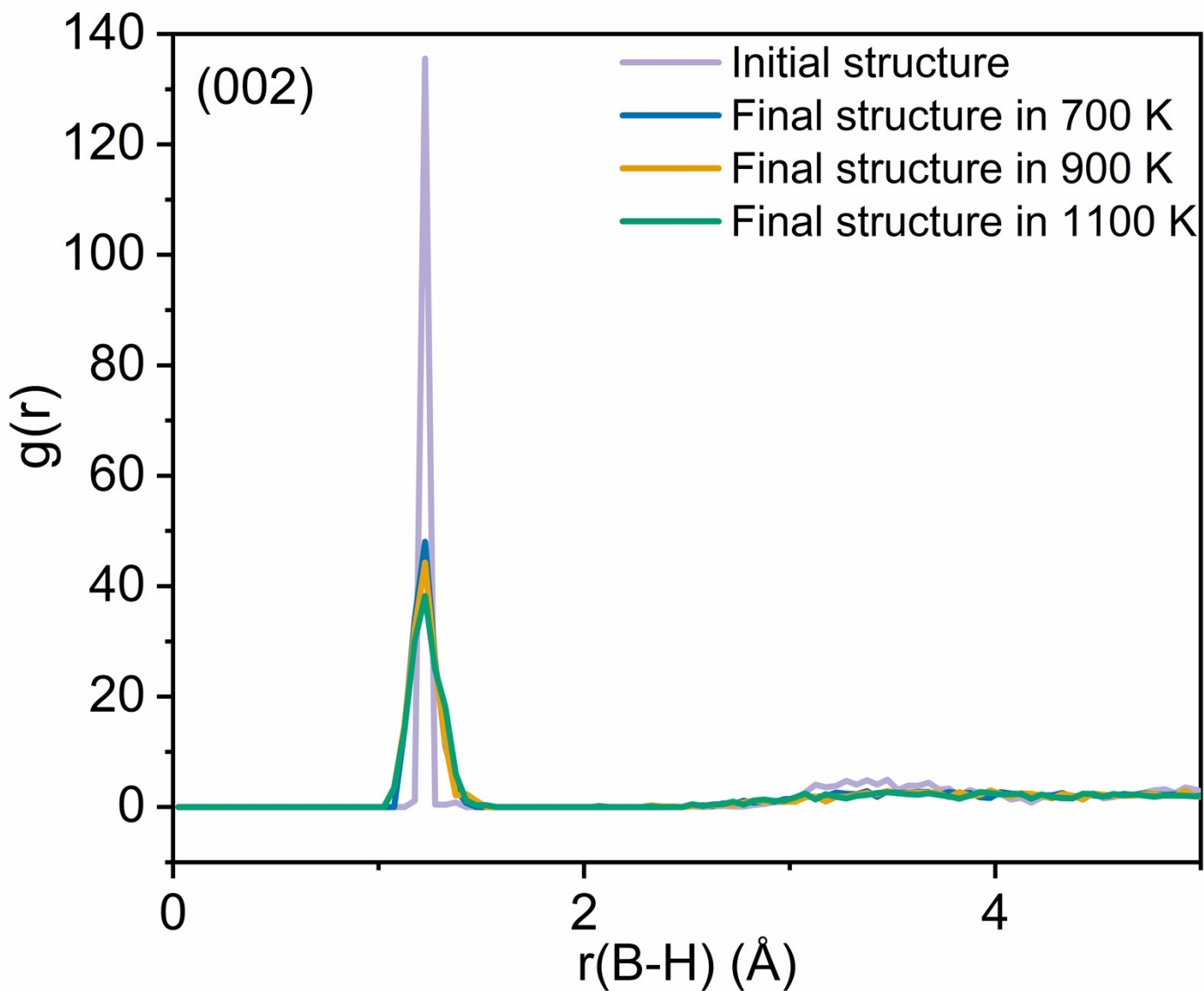
**Fig. S2** The MSD curves of hydrogen atoms at different temperatures for the  $\text{LiBH}_4$  (011).



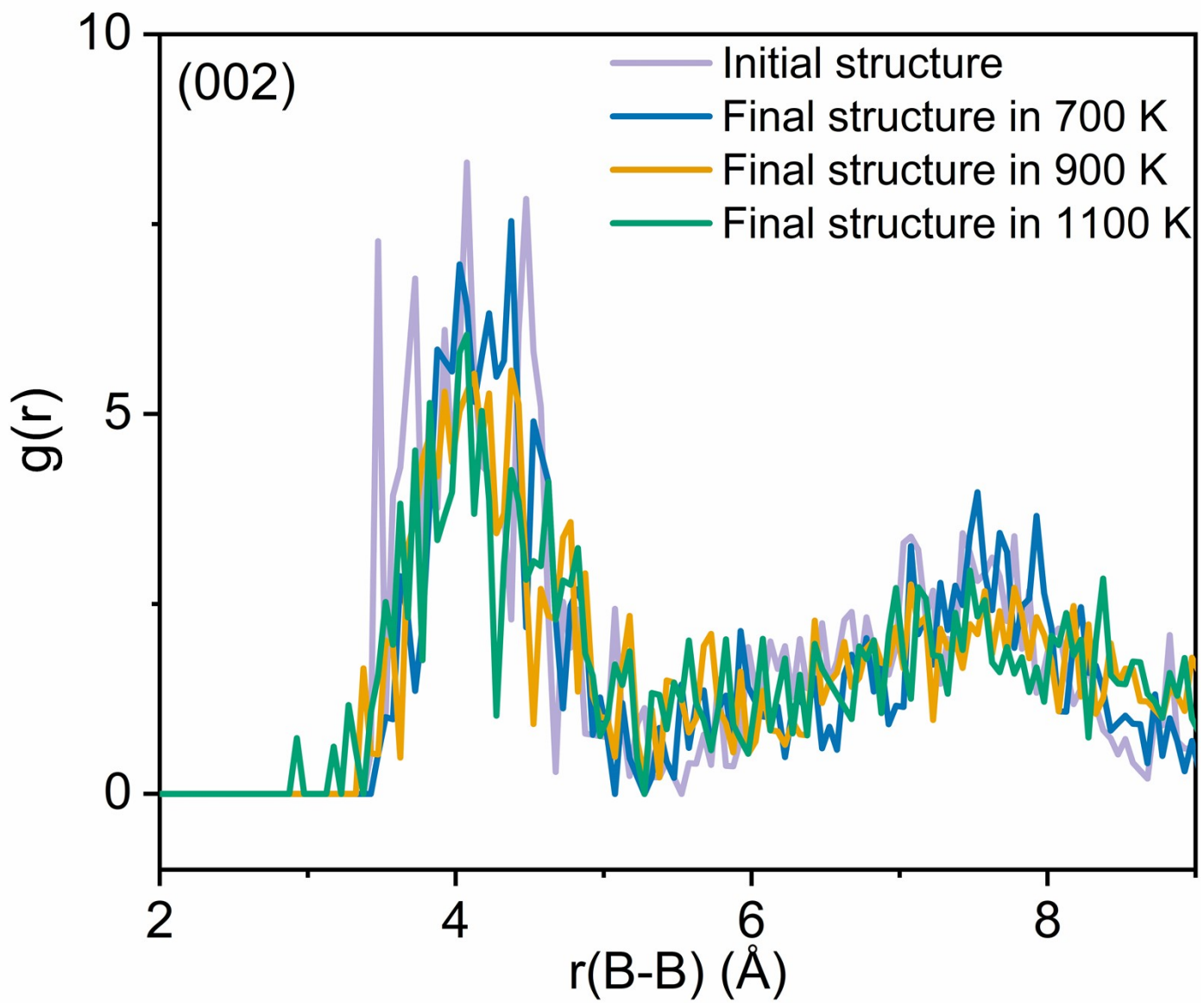
**Fig. S3** The MSD curves of hydrogen atoms at different temperatures for the  $\text{LiBH}_4$  (020).



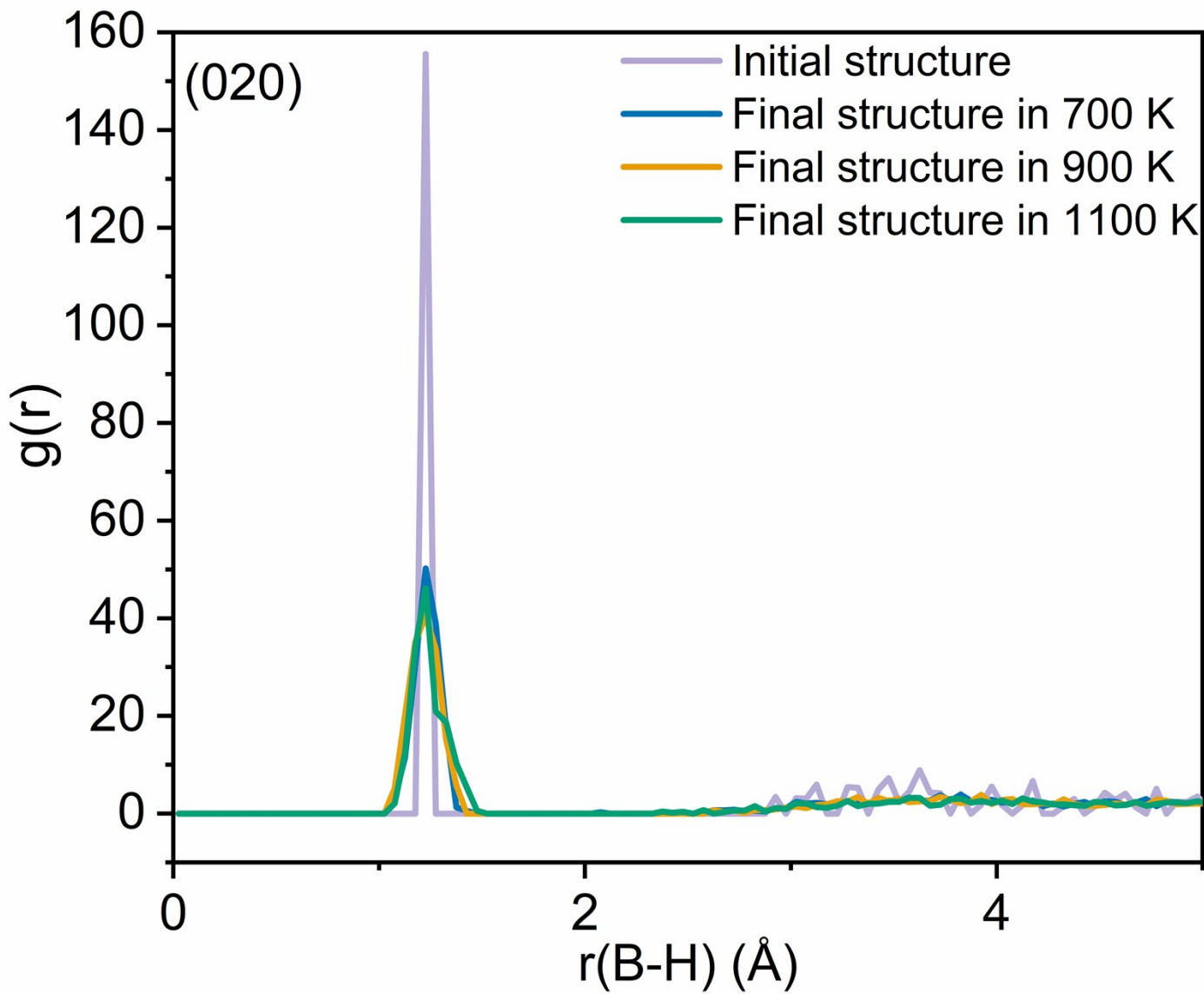
**Fig. S4** The MSD curves of hydrogen atoms at different temperatures for the  $\text{LiBH}_4$  (200).



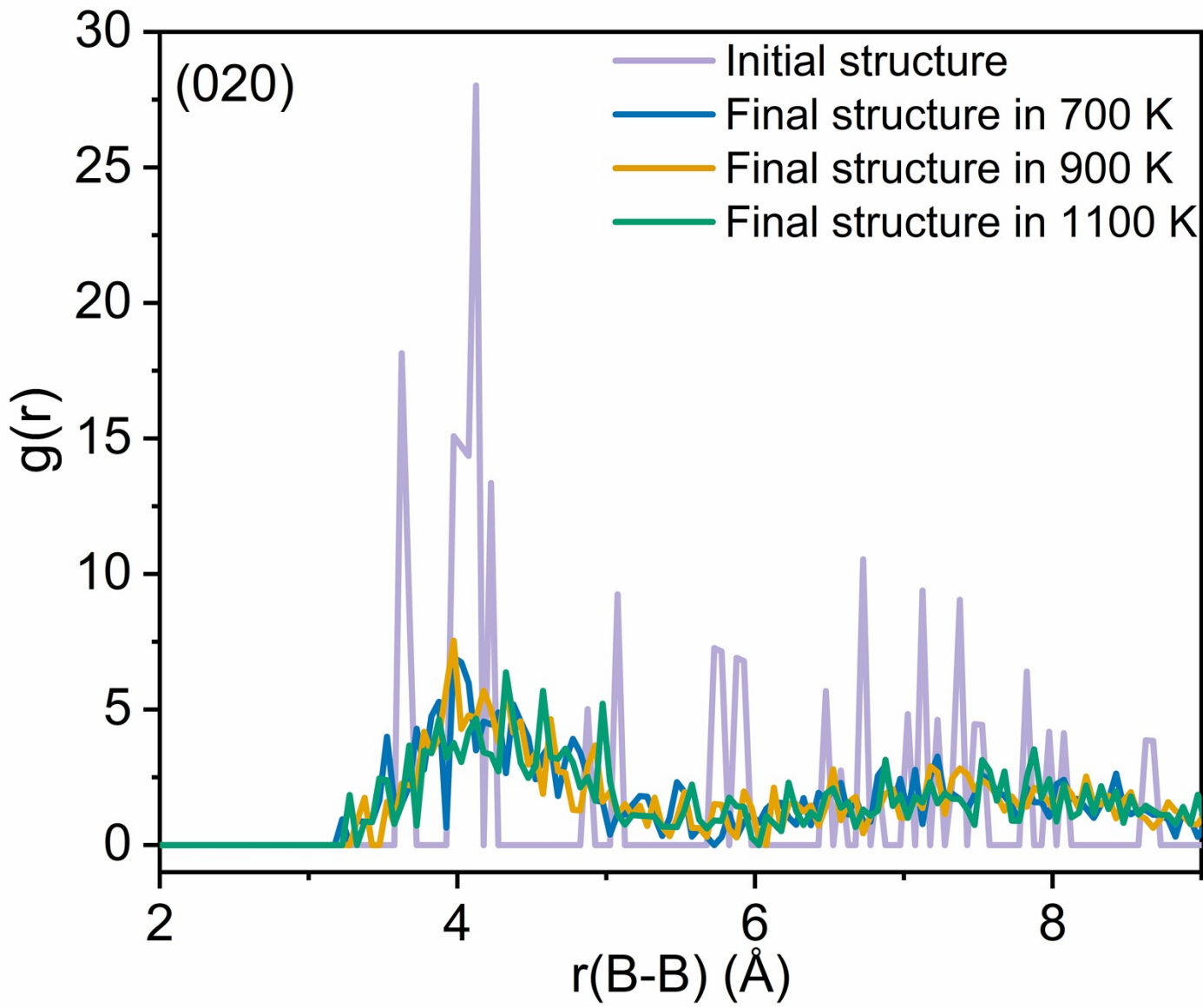
**Fig. S5** RDF of B-H of initial and final structures of 10000fs at different temperatures for the  $\text{LiBH}_4$  (002) surface.



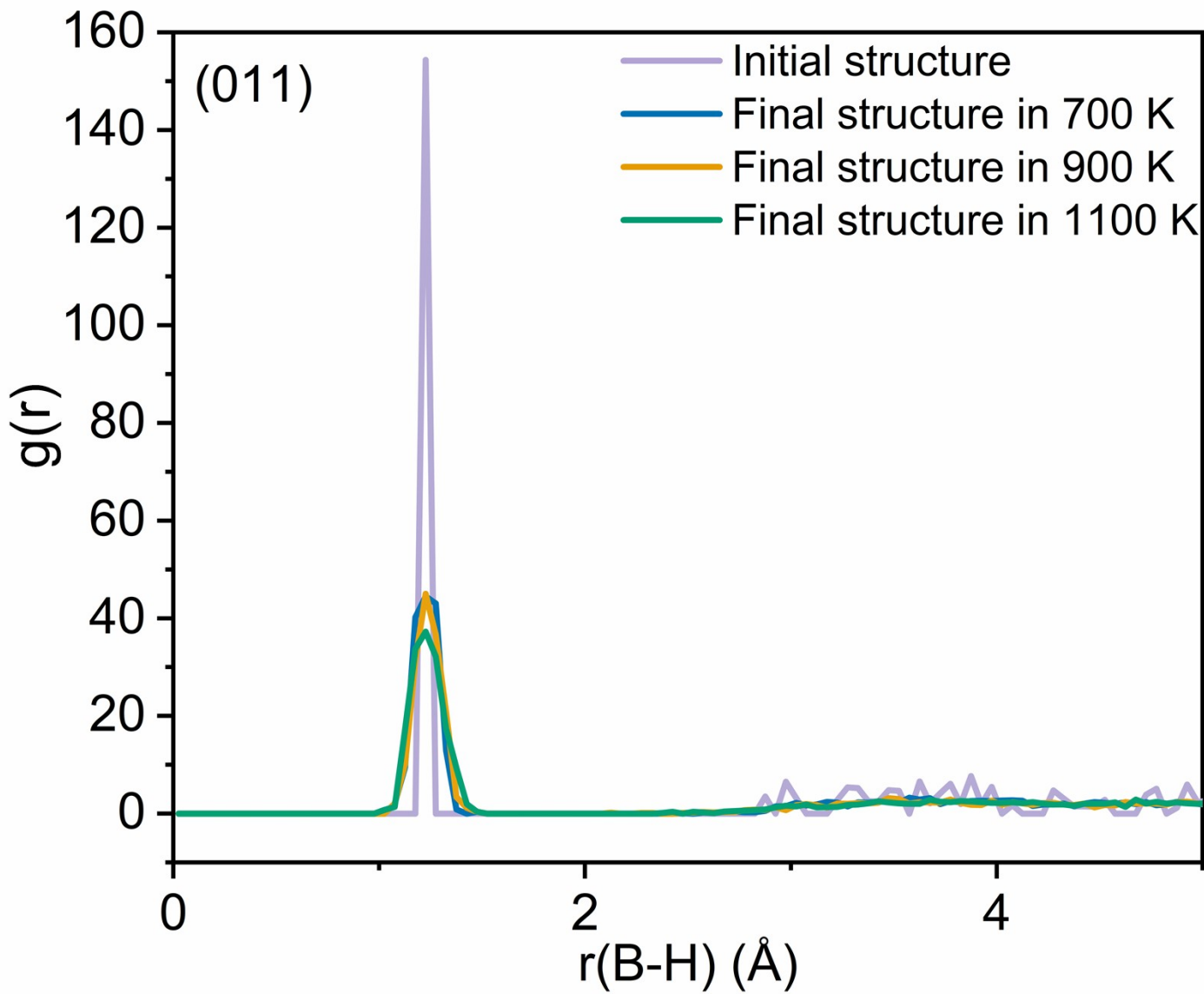
**Fig. S6** RDF of B-B of initial and final structures of 10000fs at different temperatures for the LiBH<sub>4</sub> (002) surface.



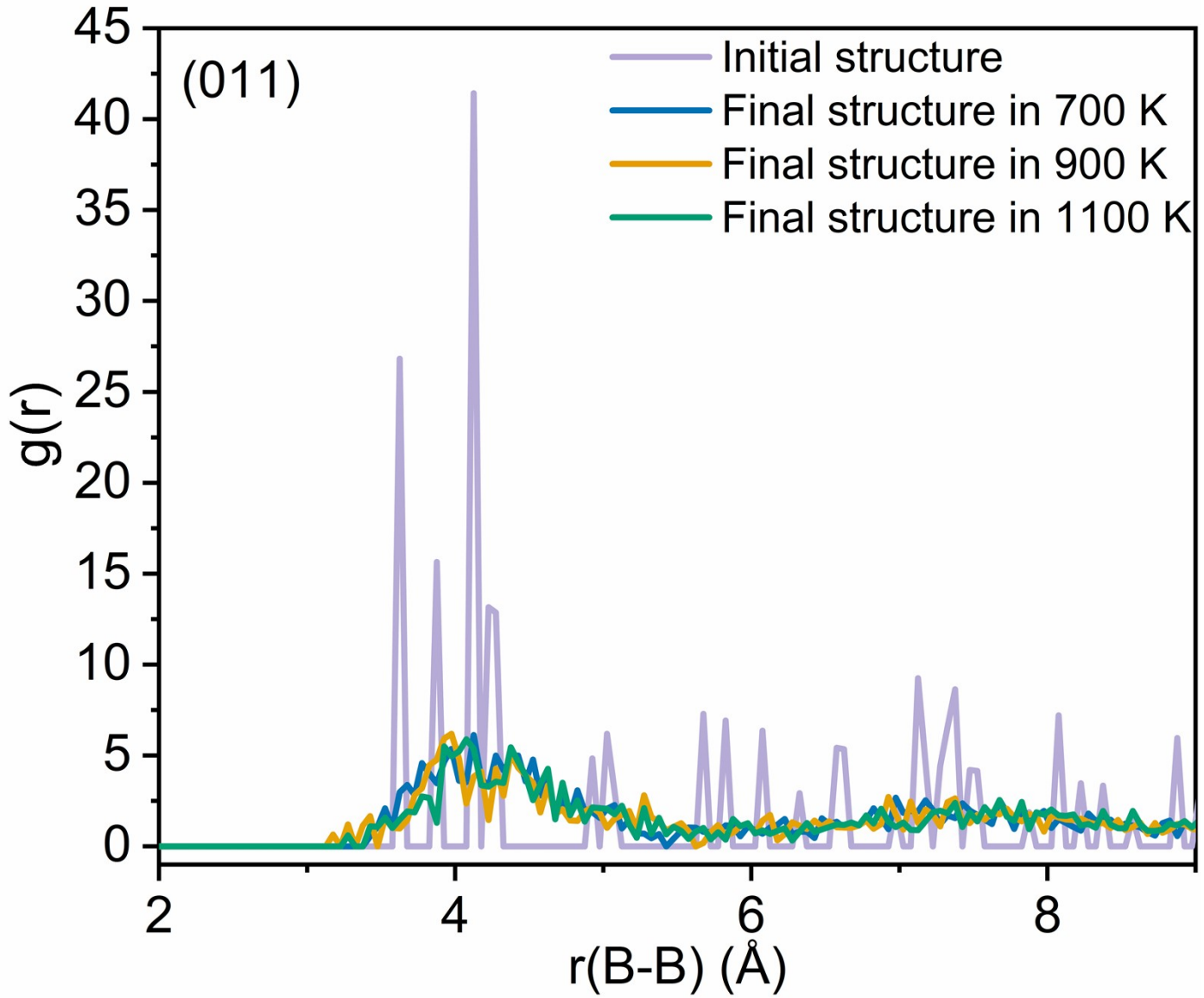
**Fig. S7** RDF of B-H of initial and final structures of 10000fs at different temperatures for the LiBH<sub>4</sub> (020) surface.



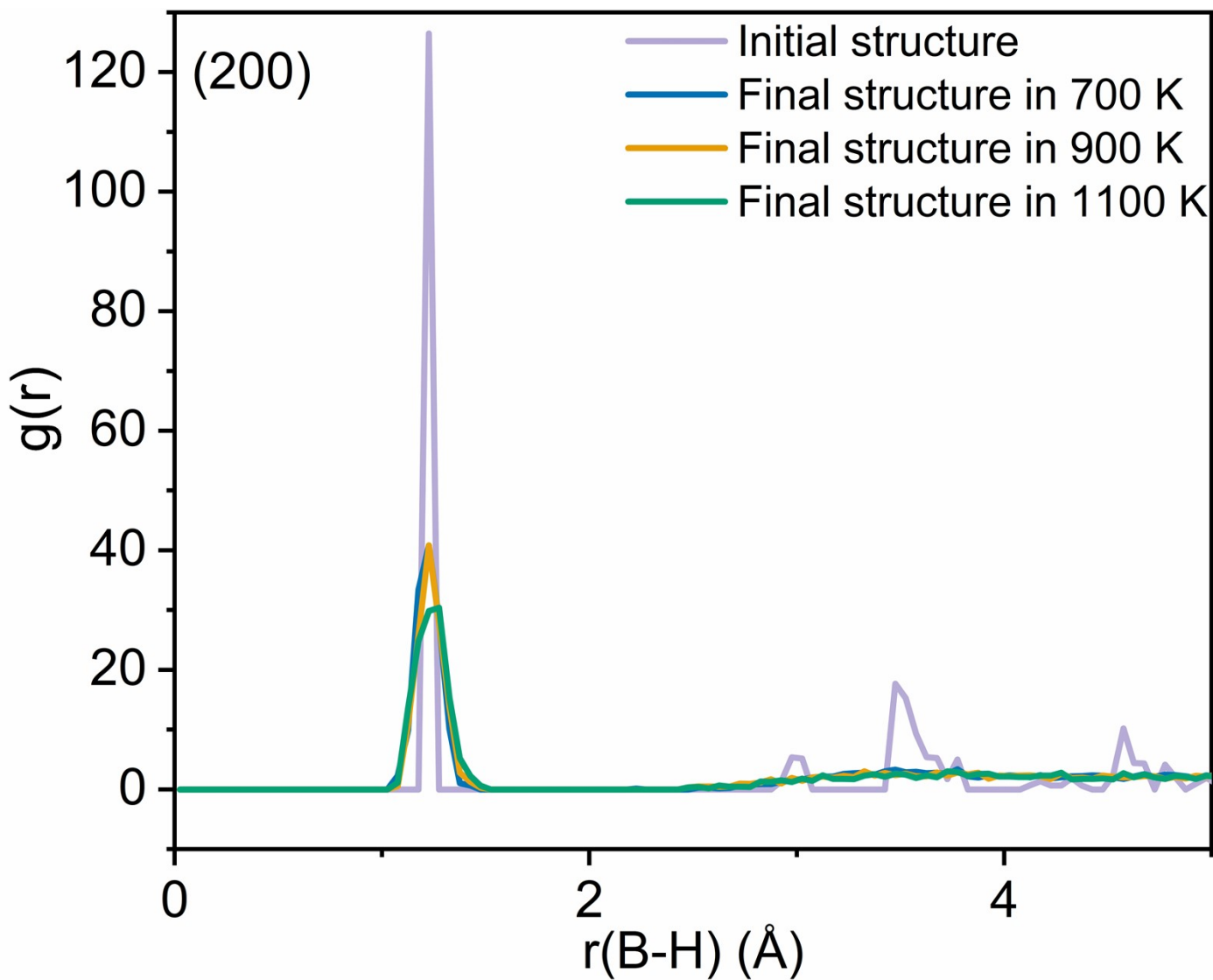
**Fig. S8** RDF of B-B of initial and final structures of 10000fs at different temperatures for the LiBH<sub>4</sub> (020) surface.



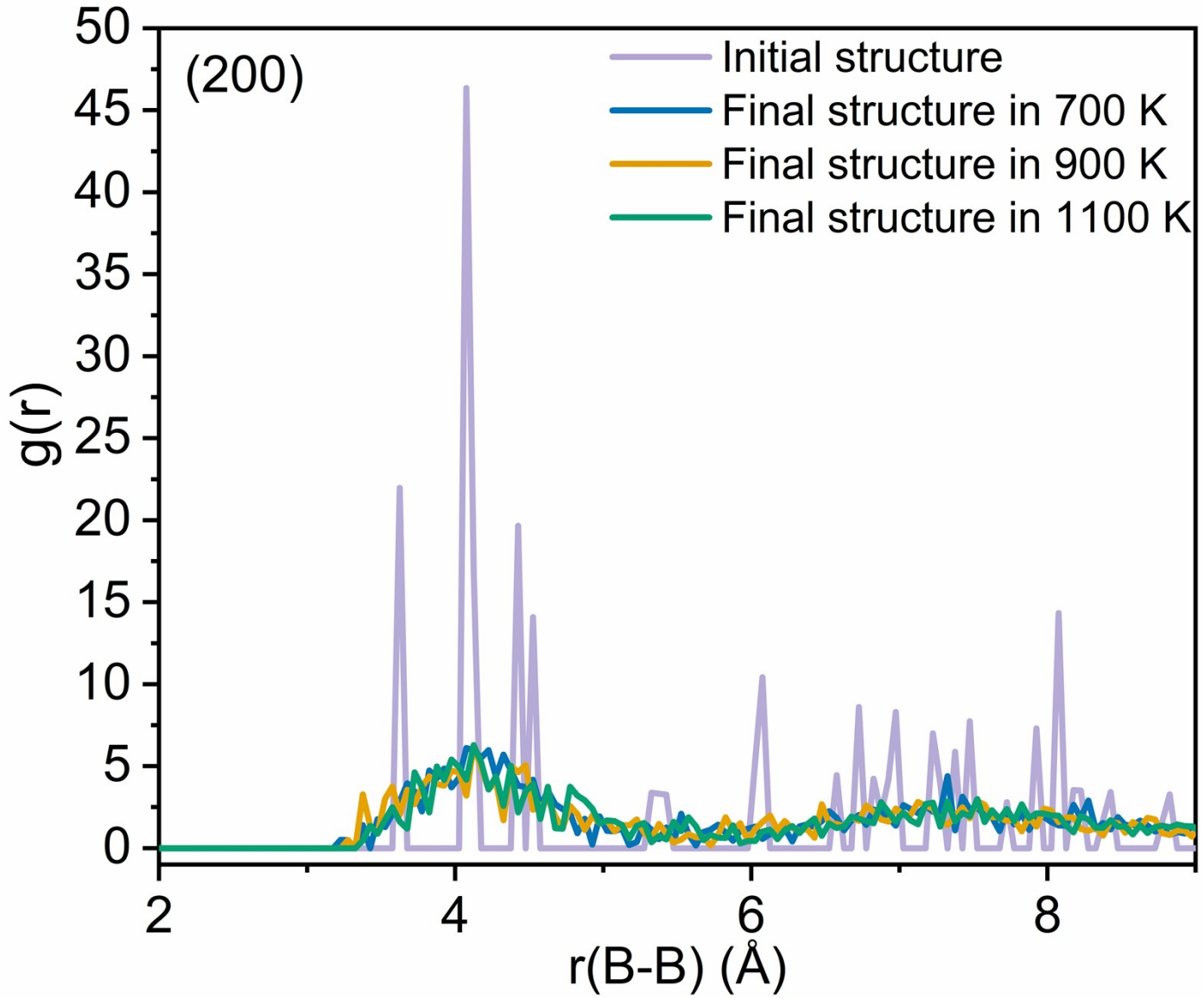
**Fig. S9** RDF of B-H of initial and final structures of 10000fs at different temperatures for the  $\text{LiBH}_4$  (011) surface.



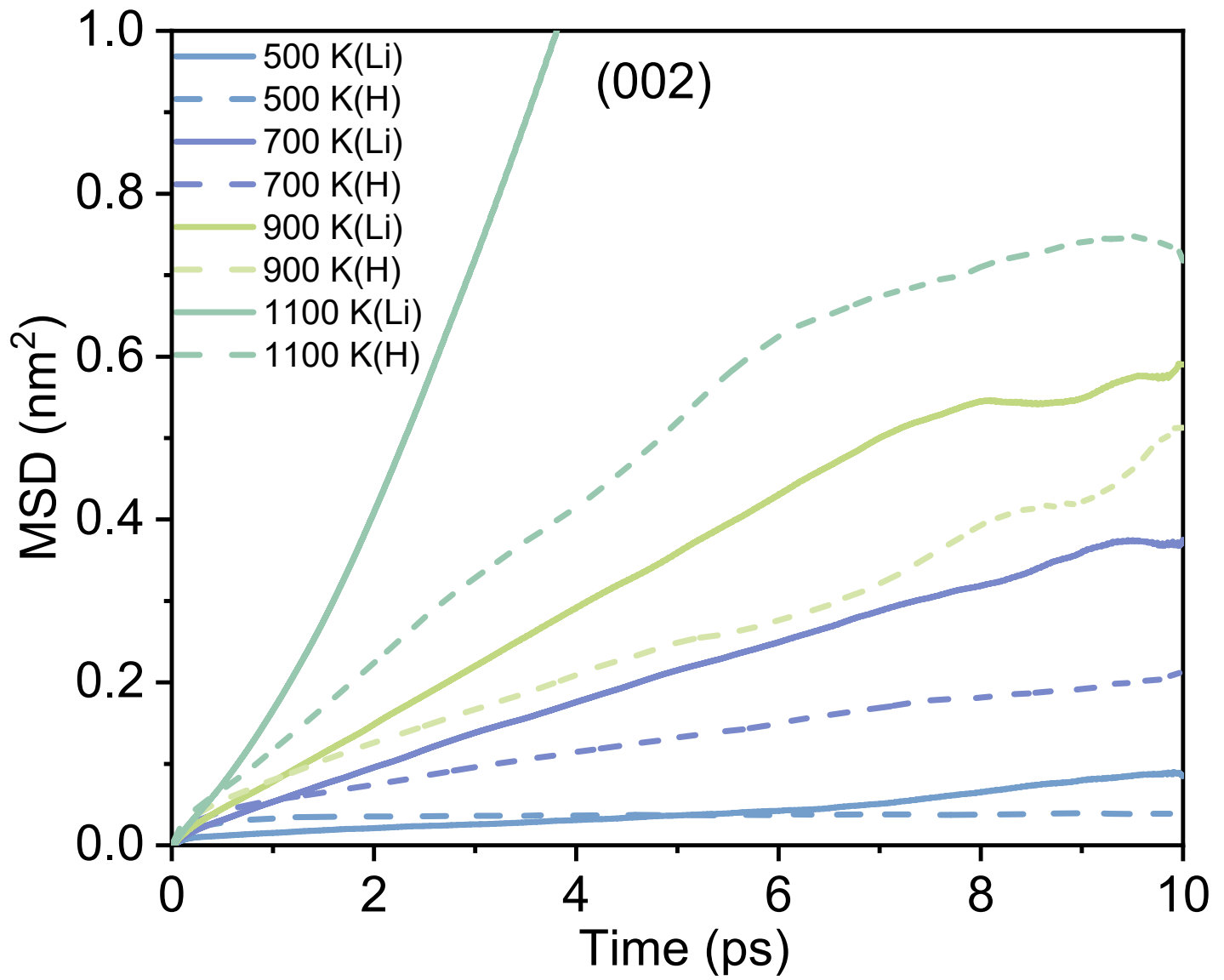
**Fig. S10** RDF of B-B of initial and final structures of 10000fs at different temperatures for the LiBH<sub>4</sub> (011) surface.



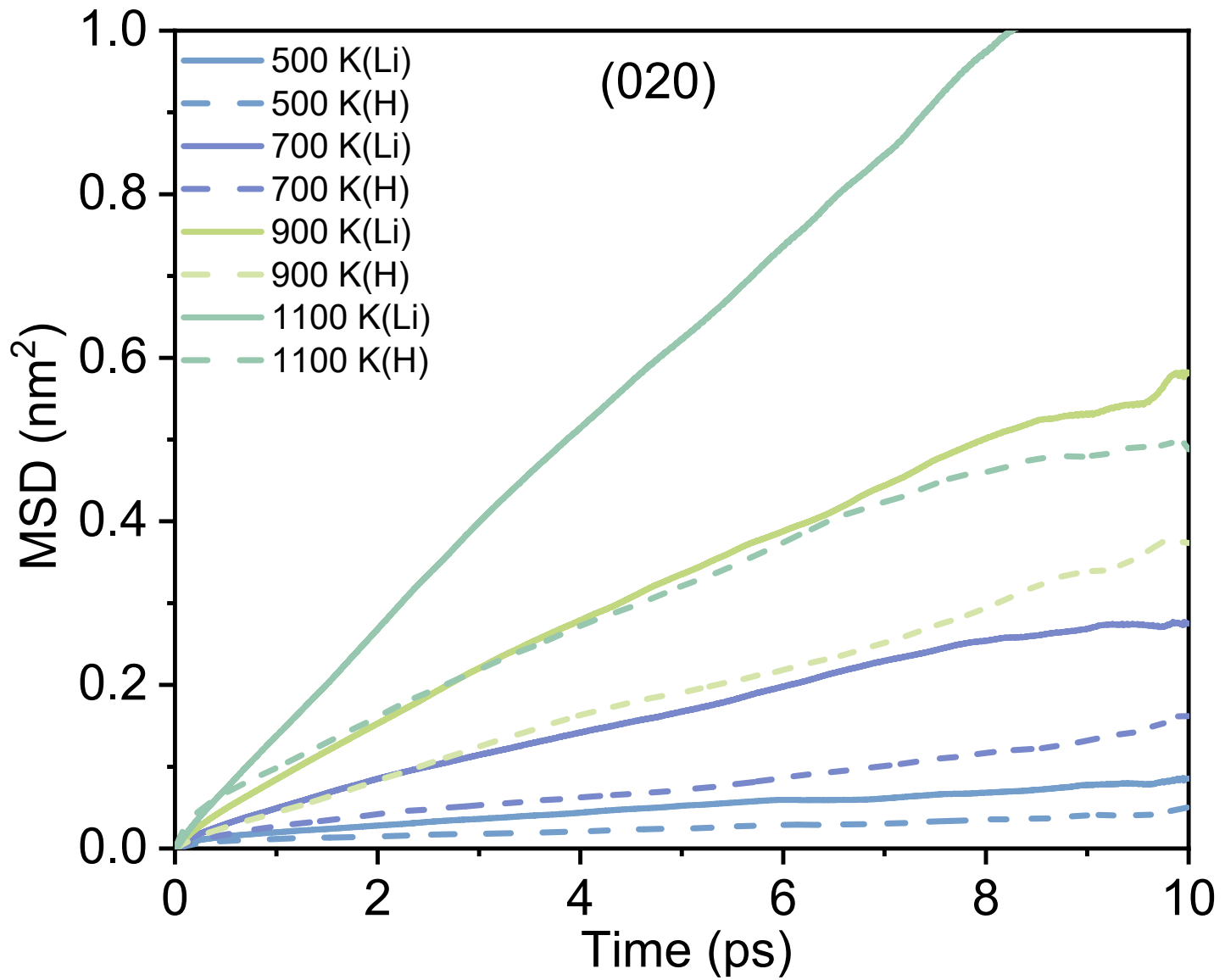
**Fig. S11** RDF of B-H of initial and final structures of 10000fs at different temperatures for the  $\text{LiBH}_4$  (200) surface.



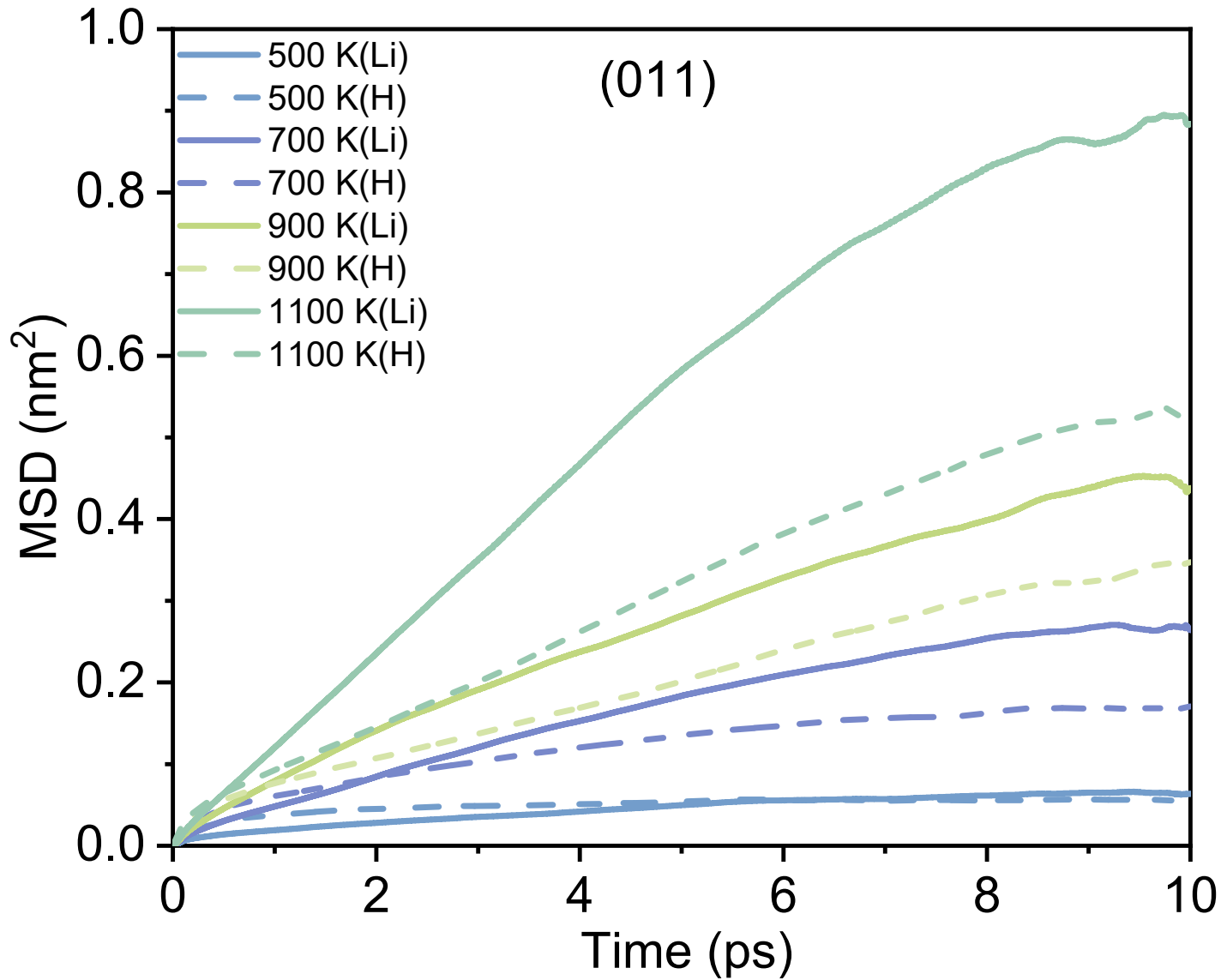
**Fig. S12** RDF of B-B of initial and final structures of 10000fs at different temperatures for the  $\text{LiBH}_4$  (200) surface.



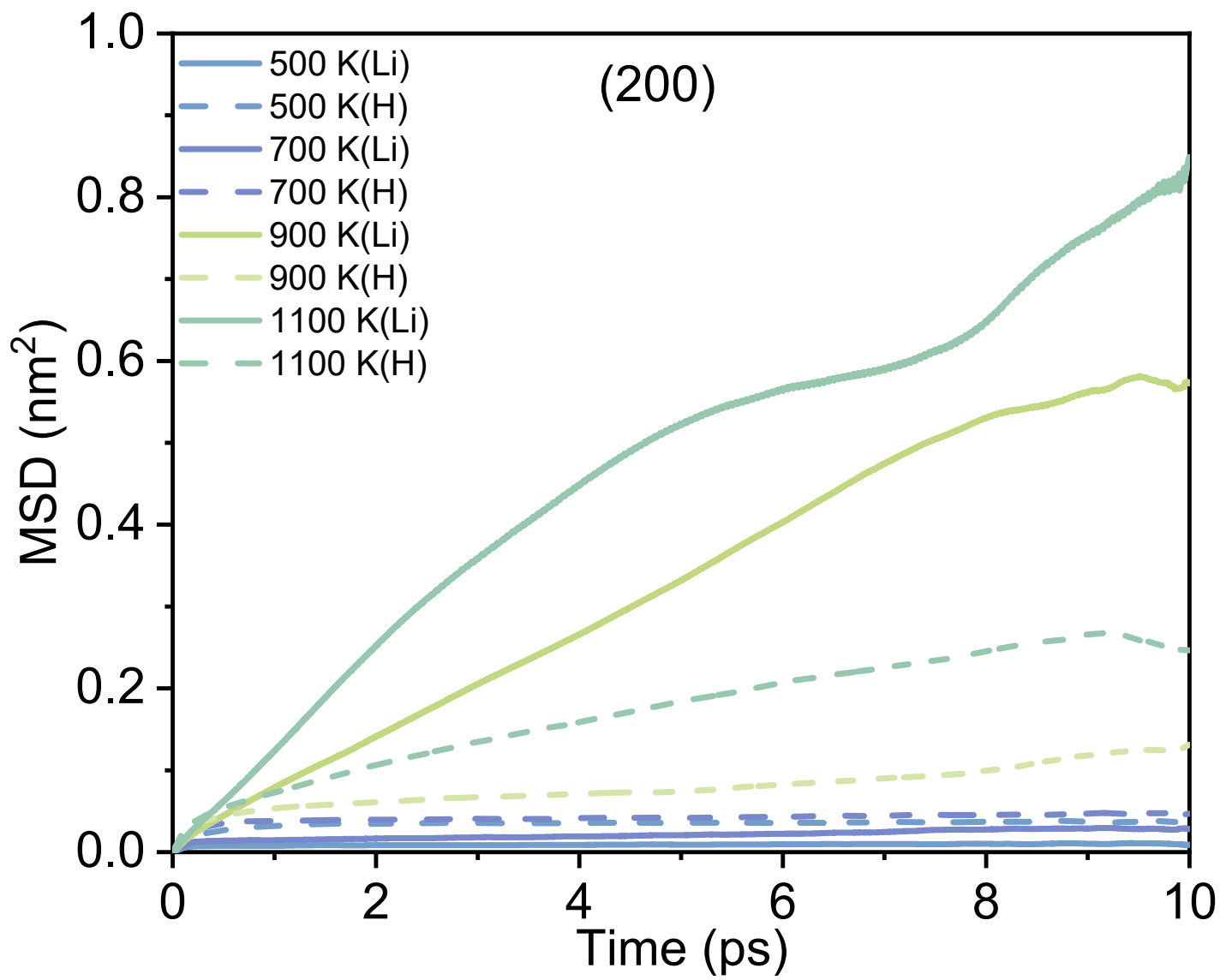
**Fig. S13** The MSD curves of both Li and H along with time at different temperatures for the (002). The dashed line represents the variation of H, while the solid line represents the variation of Li.



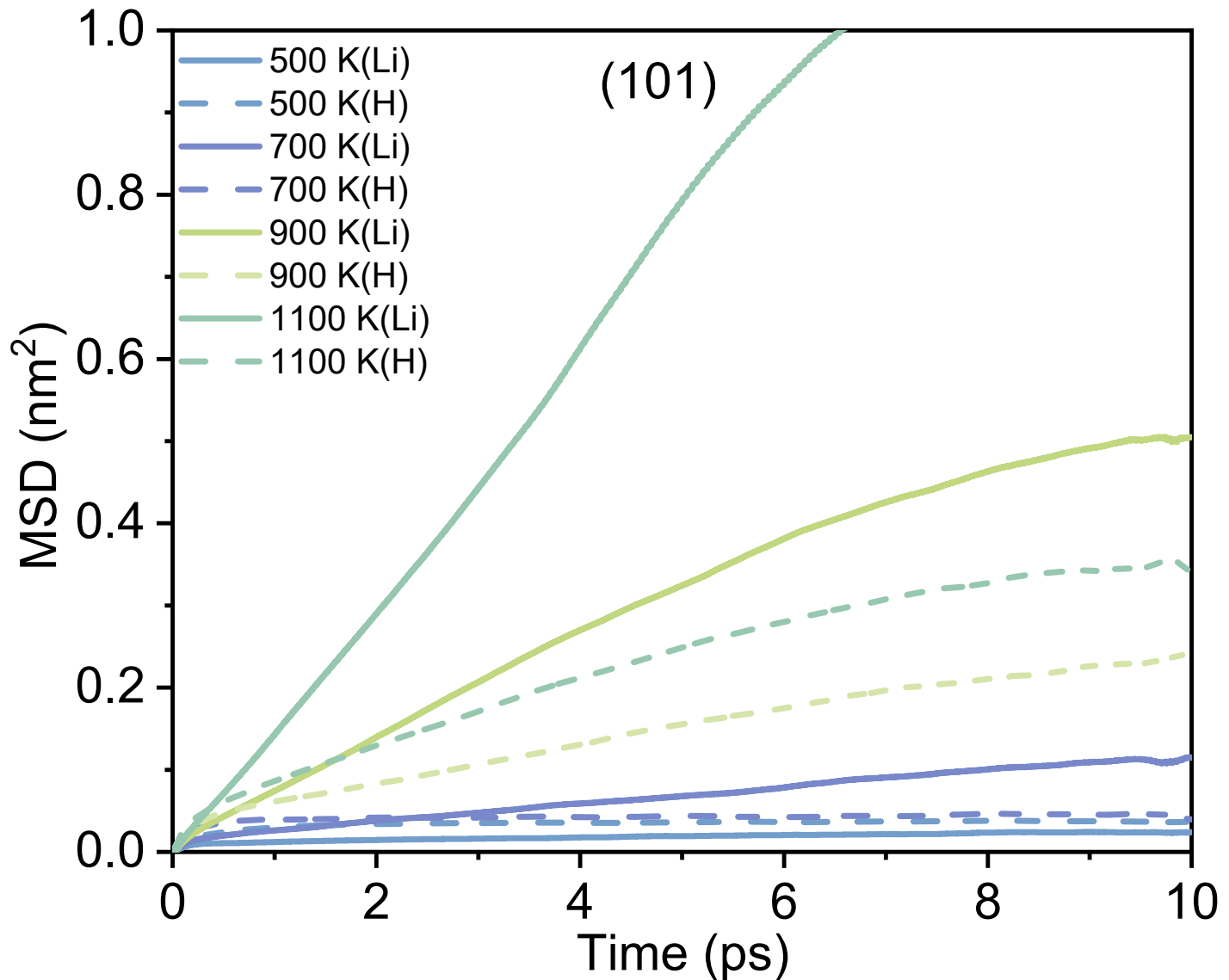
**Fig. S14** The MSD curves of both Li and H along with time at different temperatures for the (020) surface. The dashed line represents the variation of H, while the solid line represents the variation of Li.



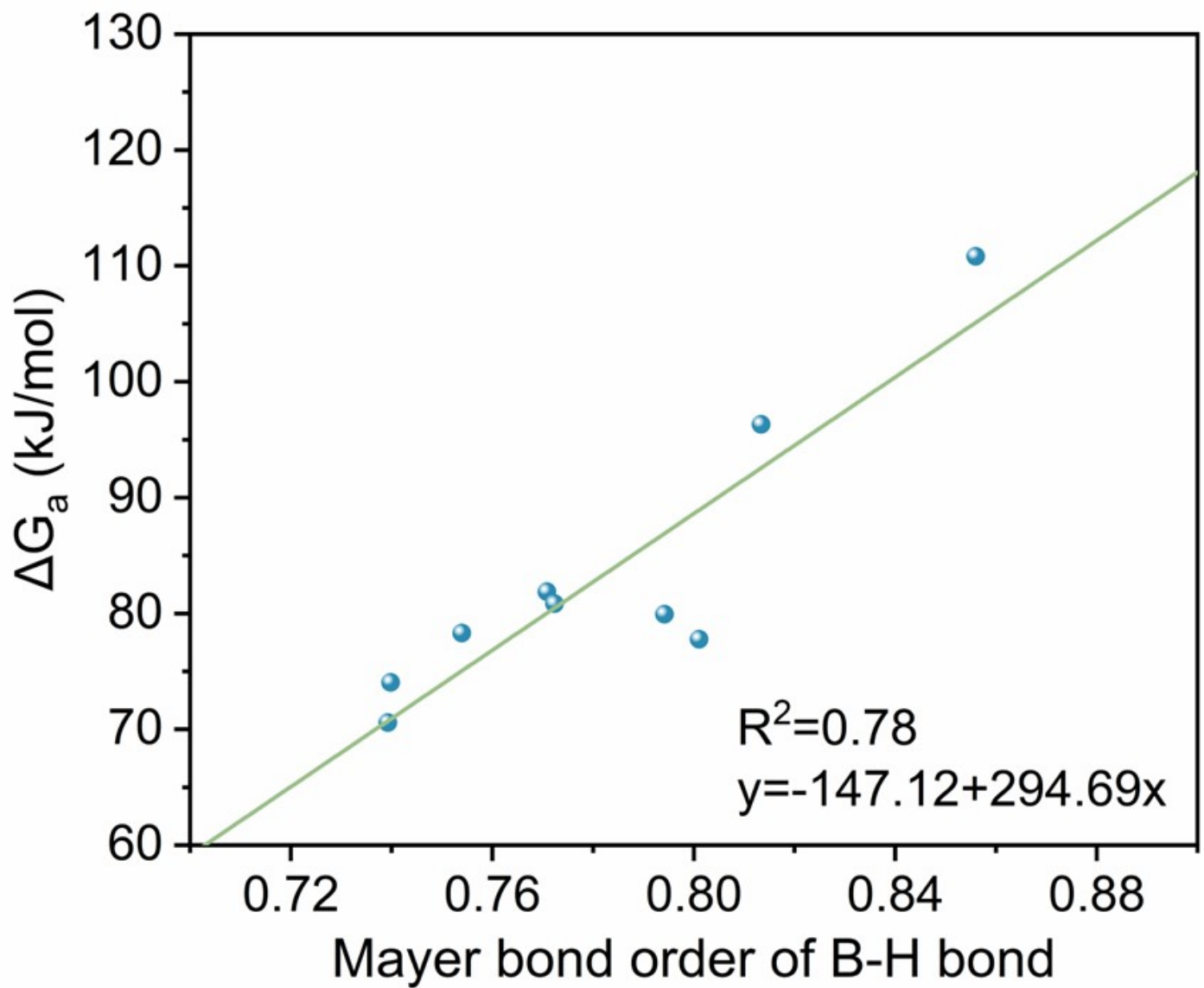
**Fig. S15** The MSD curves of both Li and H along with time at different temperatures for the (011) surface. The dashed line represents the variation of H, while the solid line represents the variation of Li.



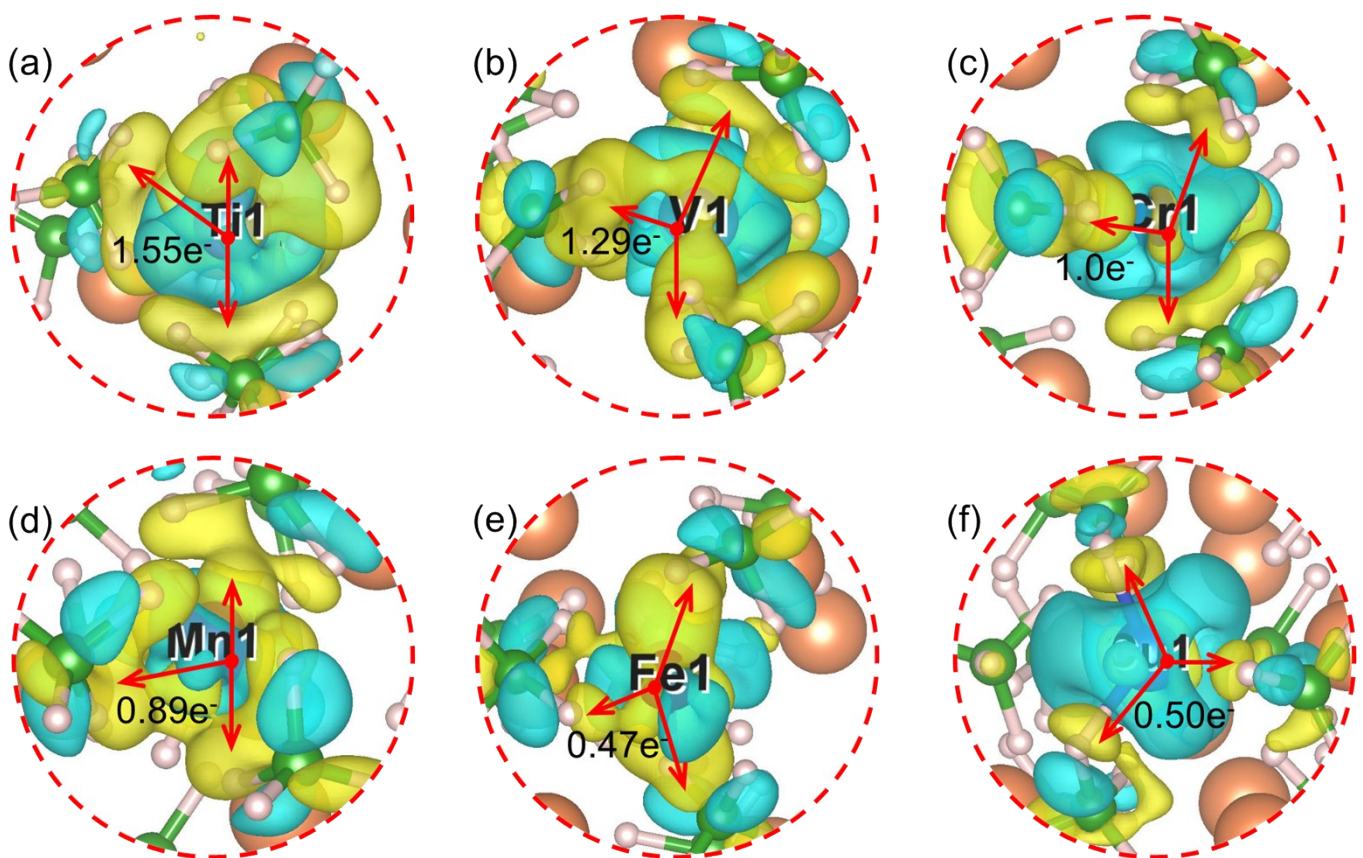
**Fig. S16** The MSD curves of both Li and H along with time at different temperatures for the (200) surface. The dashed line represents the variation of H, while the solid line represents the variation of Li.



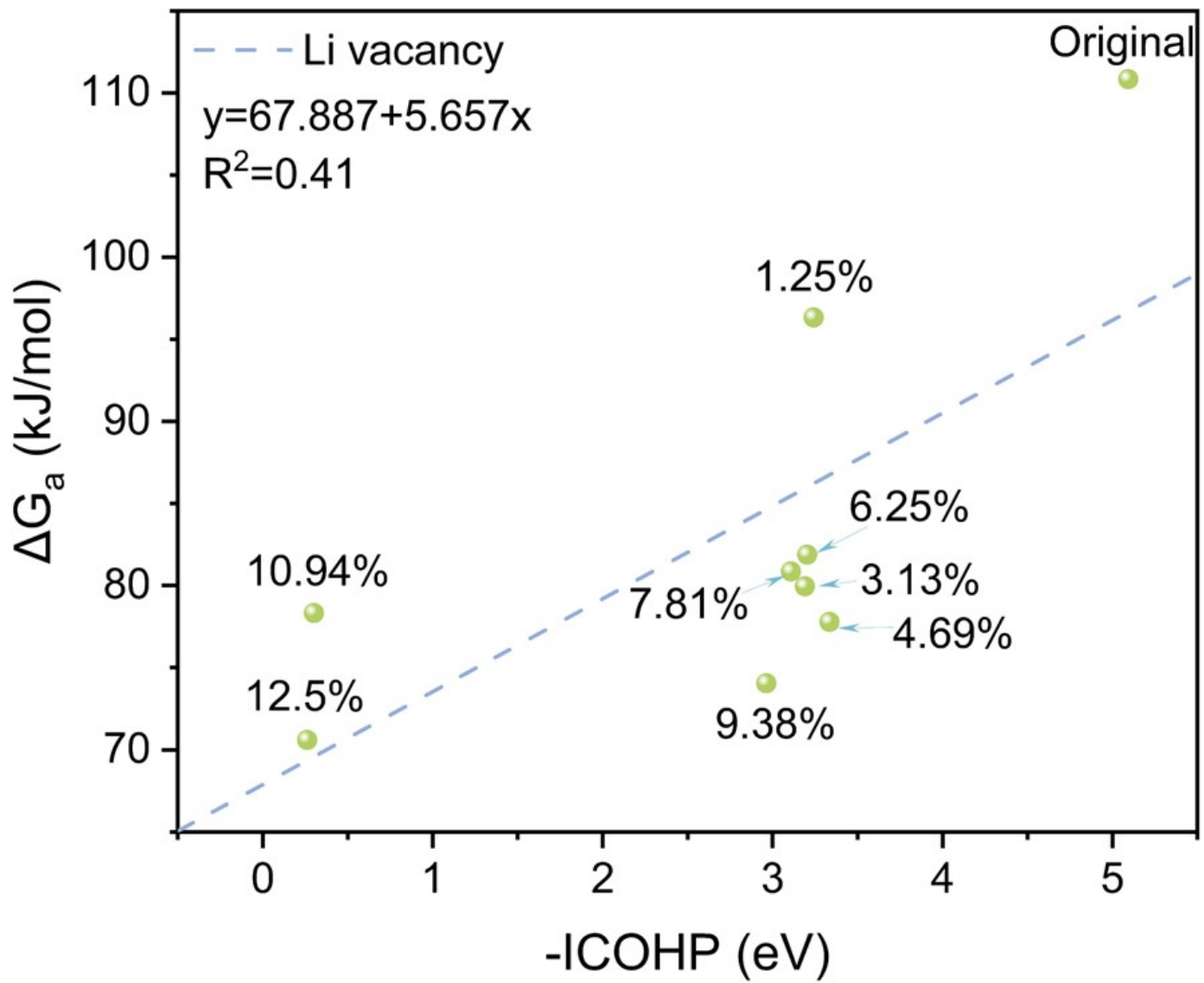
**Fig. S17** The MSD curves of both Li and H along with time at different temperatures for the (101) surface. The dashed line represents the variation of H, while the solid line represents the variation of Li.



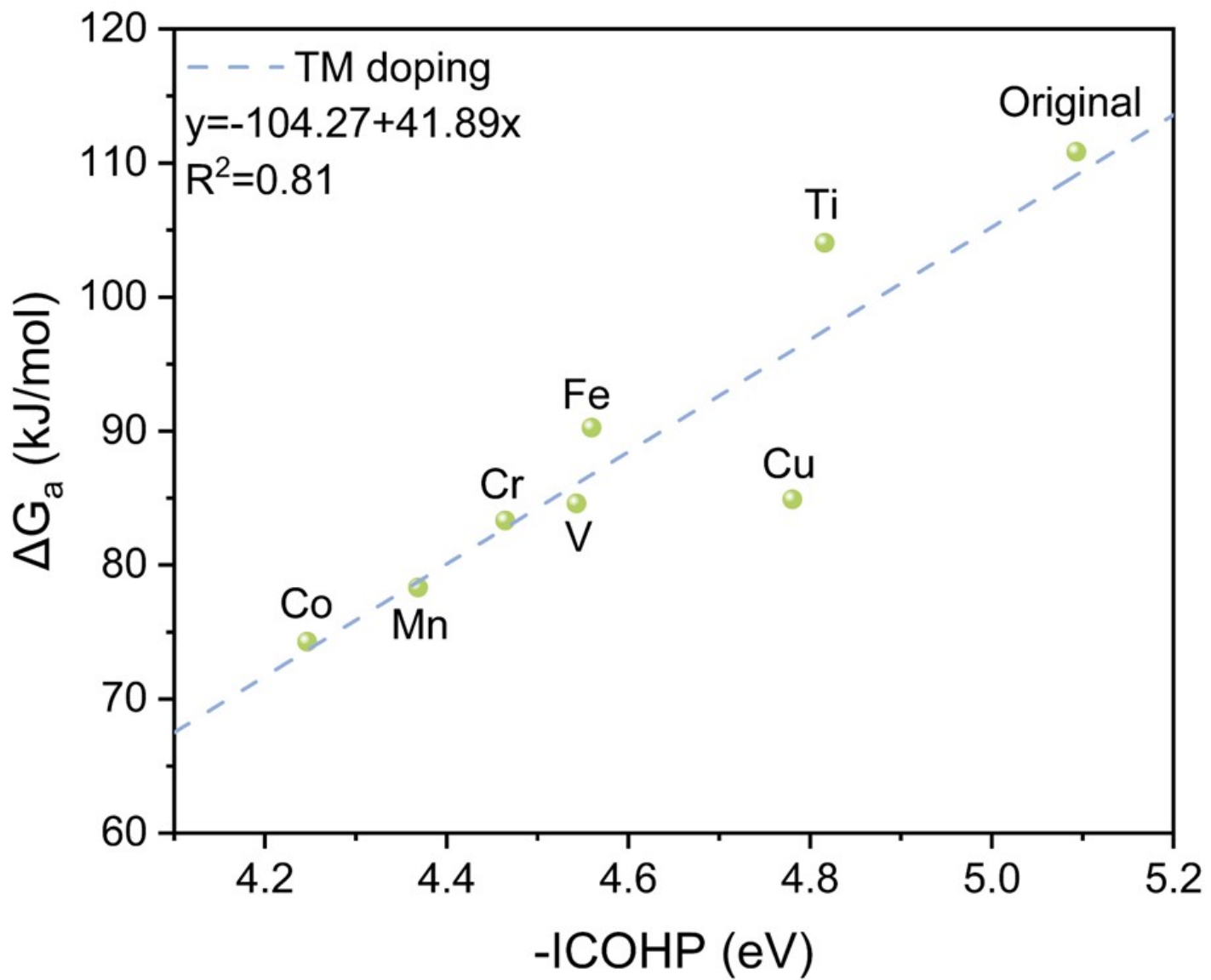
**Fig. S18** The relationship of dehydrogenation barrier of LiBH<sub>4</sub> (002) surface and Mayer average bond order of the B-H bonds in the surface layer.



**Fig. S19** Electron density difference of doped transition metal (a)-(f) Ti, V, Cr, Mn, Fe and Cu. The yellow and blue isosurface indicate electron accumulation and loss, respectively. The result is plotted with an isovalue of  $0.001 \text{ e } \text{\AA}^{-3}$ , the red dot represents the position of transition metals and the red arrows represent the direction of electron transfer, white, yellow and green spheres represent H, Li, and B respectively.

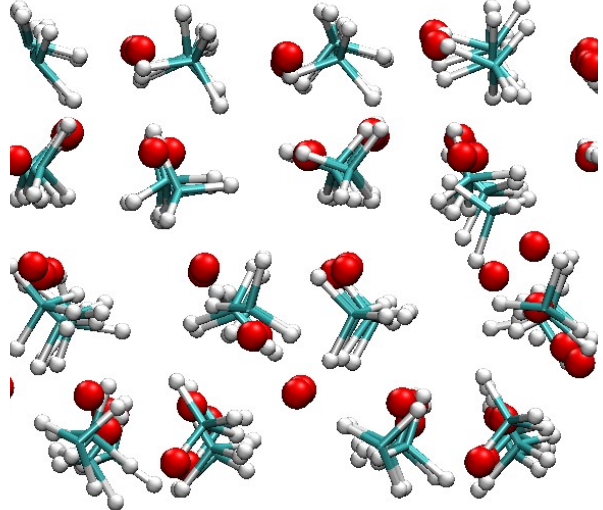
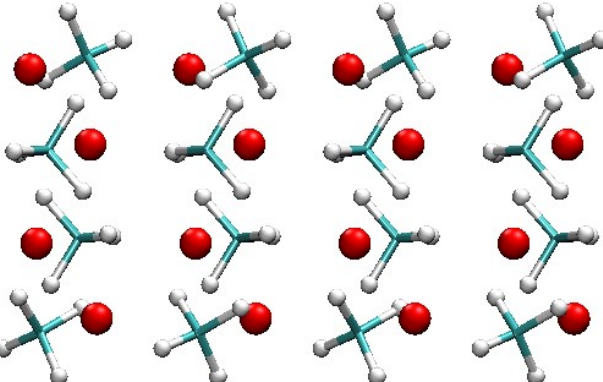
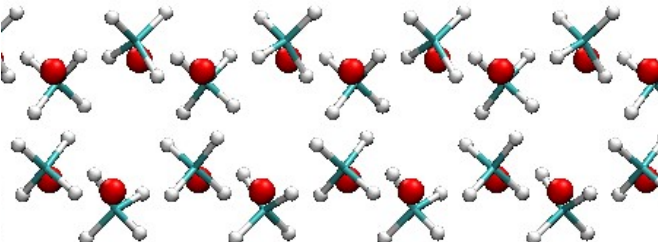


**Fig. S20** The relationship between dehydrogenation barrier of  $\text{LiBH}_4$  (002) and -ICOHP in the system of Li vacancy.

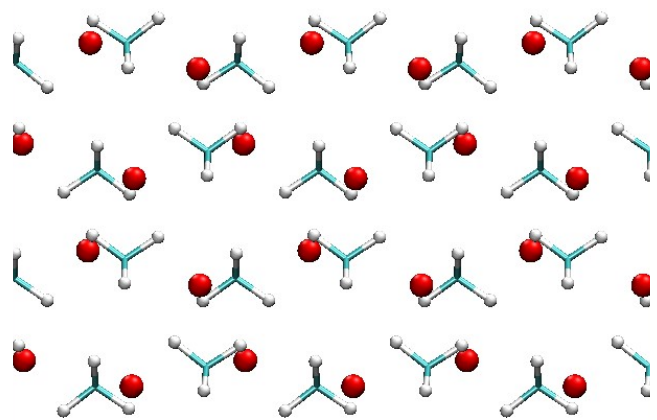


**Fig. S21** The relationship between dehydrogenation barrier of  $\text{LiBH}_4$  (002) and -ICOHP in the system of TM doping.

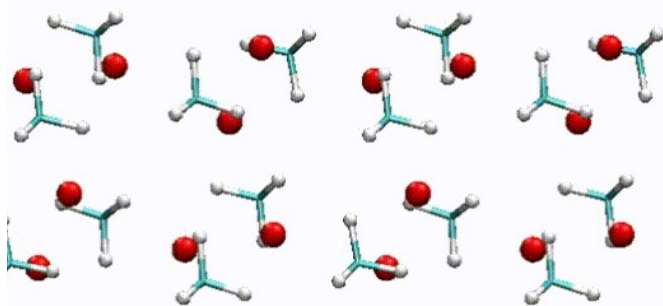
**Table. S6** AIMD simulation dynamic graphs of different surfaces of LiBH<sub>4</sub>

Surface	Movies
(002)	
(020)	
(011)	

(200)



(101)



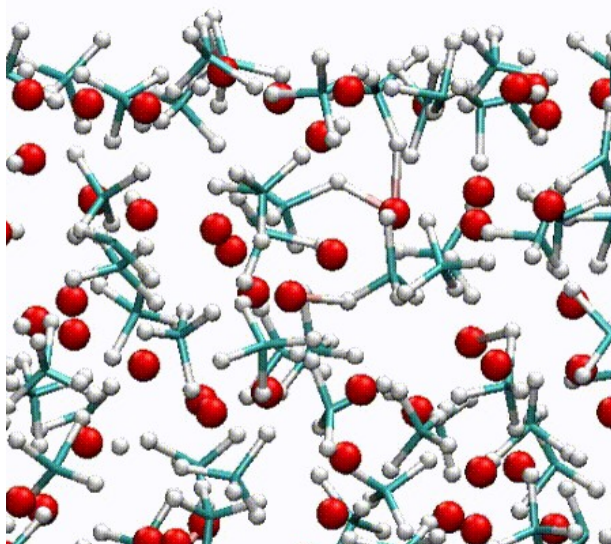
**Note:** the red sphere is Li, the connection of the green stick is B (for the convenience of highlighting the movement of H and Li, B is not displayed in a sphere), and the white sphere is H.

**Table. S7** MD simulation dynamic graphs of LiBH<sub>4</sub> (002) surface with Li vacancy

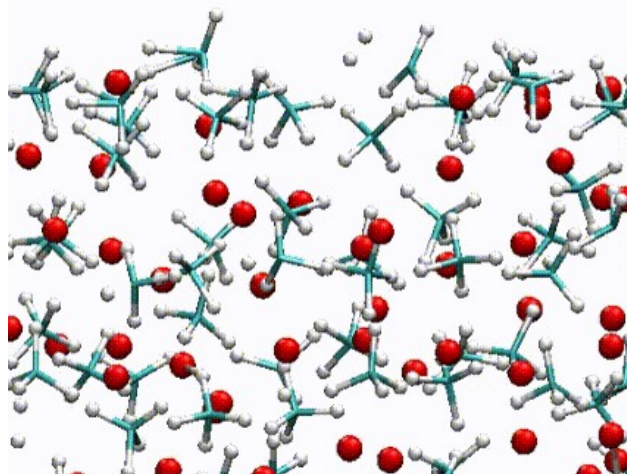
The concentration of Li vacancy

Movies

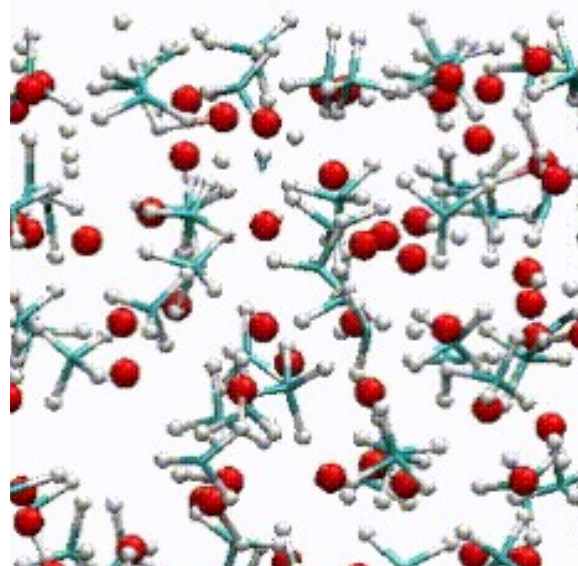
1.56%



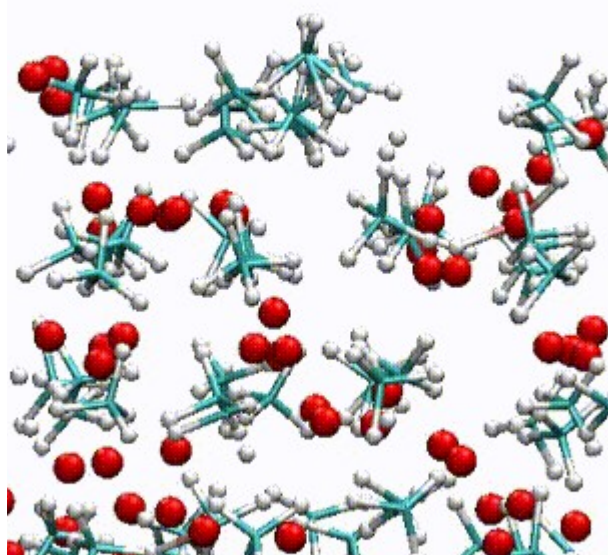
3.13%



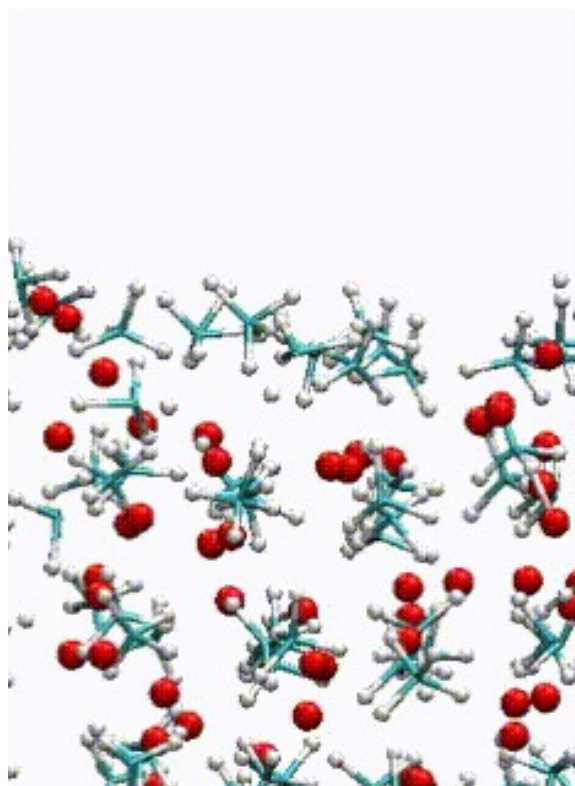
4.69%



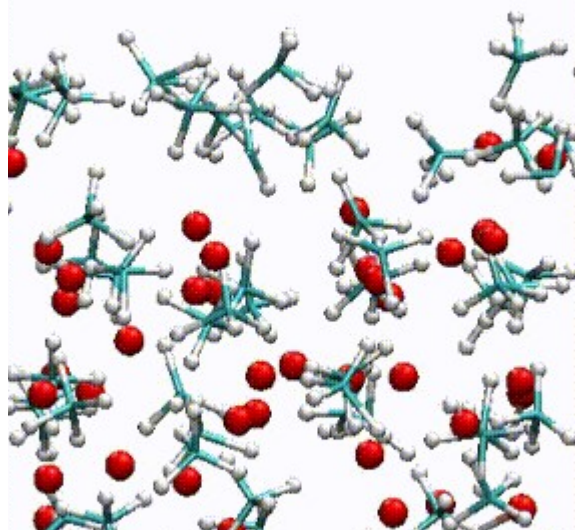
6.25%



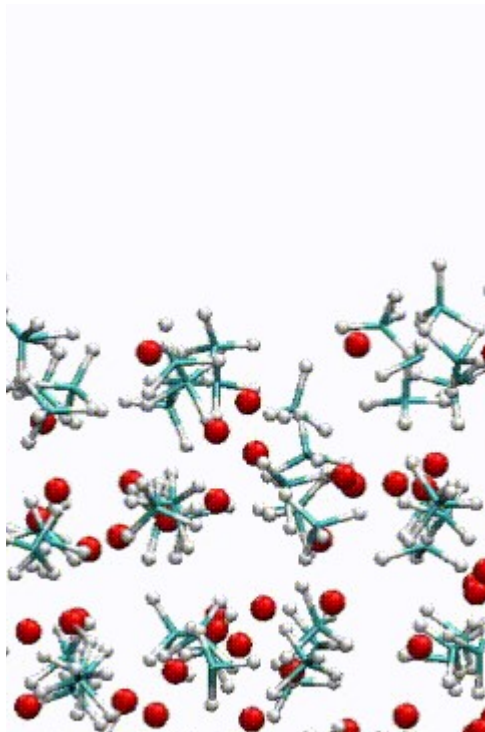
7.81%



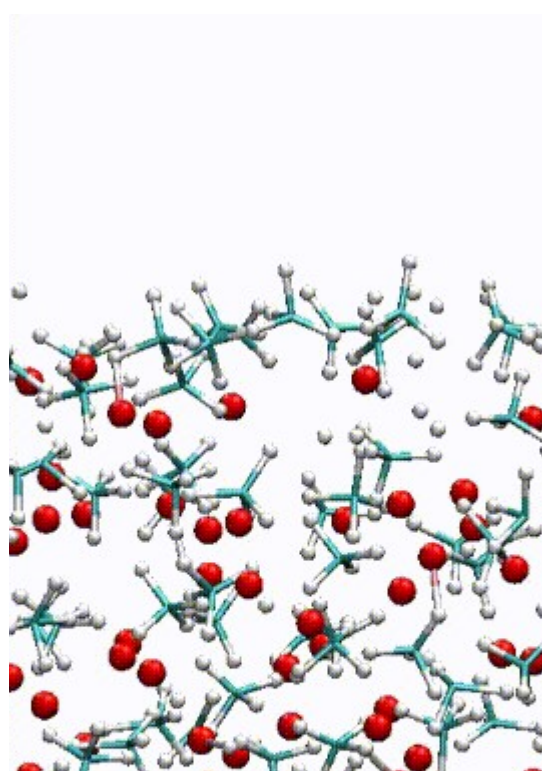
9.38%



10.94%



12.5%



---

Note: the red sphere is Li, the connection of the green stick is B (for the convenience of highlighting the movement of H and Li, B is not displayed in a sphere), and the white sphere is H.

## References

- 1 A. Züttel, S. Rentsch, P. Fischer, P. Wenger, P. Sudan, P. Mauron and C. Emmenegger, *Journal of Alloys and Compounds*, 2003, **356-357**, 515-520.
- 2 J. K. Kang, S. Y. Kim, Y. S. Han, R. P. Muller and W. A. Goddard, III, *Applied Physics Letters*, 2005, **87**, 111904.
- 3 J. P. Soulié, G. Renaudin, R. Černý and K. Yvon, *Journal of Alloys and Compounds*, 2002, **346**, 200-205.